Turbulence and Wave Breaking Effects on Air-Water Gas Exchange

Evelyn J. Boettcher,[1] Jay Fineberg,[1,2] and Daniel P. Lathrop[1]

[1]*Institute of Plasma Research, Department of Physics, University of Maryland, College Park, Maryland 20742*
[2]*The Racah Institute of Physics, The Hebrew University of Jerusalem, Jerusalem 91904, Israel*

We present an experimental characterization of the effects of turbulence and breaking gravity waves on air-water gas exchange in standing waves. We identify two regimes that govern aeration rates: turbulent transport when no wave breaking occurs and bubble dominated transport when wave breaking occurs. In both regimes, we correlate the qualitative changes in the aeration rate with corresponding changes in the wave dynamics. In the latter regime, the strongly enhanced aeration rate is correlated with measured acoustic emissions, indicating that bubble creation and dynamics dominate air-water exchange.

The air-water gas exchange between the atmosphere and the ocean takes place on a grand scale. For example, the oceans hold 60 times more dissolved carbon ($\sim 38\,000$ gigatons) than the atmosphere and 38 times more than the total vegetative carbon reservoir on land [1]. The oceanic absorption of atmospheric gases (including CO_2 and CH_4) plays an important role in climate modeling and prediction [2]. Air-water gas exchange is also important in man-made systems. For instance, in waste water treatment where bioremediation is used in large man-made water reservoirs, proper aeration is needed for aerobic breakdown of waste material.

The wave state strongly affects air-water gas exchange. Factors such as turbulence below the surface, wave breaking, and the velocity field of the fluid affect the rate of ingassing. Extensive studies of the mass transport of atmospheric gases and trace gases into water have been carried out. These studies can be grouped into three types of experiments: Faraday excited capillary waves [3,4], wind driven waves [4–6], and field data in nature [7]. Large wave systems, such as the oceans, tend to be gravity wave dominated. Wind driven waves in the ocean cause enhanced ingassing from the waves and from thermal currents fueled by evaporation. In this Letter, we address how breaking waves and wave turbulence affect the rate of ingassing for standing gravity waves.

We first address wave states in which no wave breaking occurs (so that the fluid surface remains simply connected). In this regime, we show that turbulent fluid transport dominates the air-water gas exchange rate. We then consider fluid-states where wave breaking occurs (i.e., the fluid surface is multiply connected with droplets and spray). We demonstrate that when wave breaking occurs, aeration through the fluid surface is significantly enhanced. We further show that bubble dynamics, characterized by acoustic measurements, become the *dominant* mechanism for air-water gas exchange.

Our experimental apparatus consists of a 2.3-m-diameter cylinder partially filled with filtered water to a depth of 1 m. A cylindrical plunger, driven by 12 linear actuators along the tank's circumference, is oscillated in the vertical direction to create gravity waves in a controlled manner (Fig. 1). The system is driven with a sinusoidal force at a single driving frequency f. The power to the plungers is continuously monitored. In this paper, we restrict the discussion of the dynamics to wave states resulting from driving the system at two distinct resonant frequencies, 1.63 and 1.82 Hz. These frequencies have corresponding linear wave states of the cylindrical tank of $J_{3,0}$ and $J_{4,4}$, where $J_{i,j}$ are cylindrical Bessel functions with i radial and j axial nodes. Nonlinear wave states corresponding to these driving frequencies (see Fig. 1) retain, on average, the symmetries of these linear modes.

For a given input power and driving frequency, we measure the oxygen concentration as an indicator of the rate of atmospheric ingassing. We record the rate of O_2 absorbed by the water and explore its dependence on the wave state. To explore this dependence, the amount of dissolved oxygen in the water is reduced. The O_2 concentration is monitored with a dissolved oxygen meter (YSI model 58) which measures the oxygen concentration at a single spatial location in the tank. One might assume that
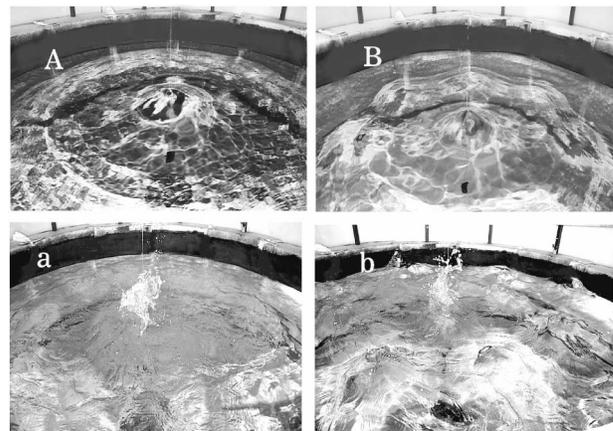

FIG. 1. Photographs show two resonant frequencies: J_{30} at $f = 1.63$ Hz (left) and J_{44} at $f = 1.82$ Hz (right). The top photograph shows standing waves (A) $P = 5$ W and (B) $P = 0.4$ W; the bottom photograph shows breaking waves (a) $P = 16$ W and (b) $P = 5$ W.

as long as the probe is located below the boundary-layer thickness $\tilde{z} = D/k$, where D is the molecular diffusion and k is the transport velocity (~ 100 μm in our experiment) [4], the measurements of the ingassing rates would not be affected by the meter's precise location. We have tested this at several locations in the bulk, which yield similar results. Our experiments were performed with the system under ambient atmospheric pressure. Our control and characterization of the excited wave state allows us to deconvolve how wave state variables affect air/water mass transport exchange.

For each wave state, the wave height at the center of the tank is measured with a wire ac resistance level sensor. Wave height measurements are used to characterize the temporal and spatial dynamics of the different states (Fig. 3). Simply connected states (Figs. 1 and 3a) are observed at low power as standing waves. The waves break at higher powers, causing envelopment of air bubbles and production of spray. For the resonant states that we use, we find the threshold power for wave breaking to be much lower than that predicted [8] where a broad driving spectrum was assumed. They predicted that the critical power flux per unit area P_0 for breaking waves to occur should be $\rho(\sigma g/\rho)^{3/4}$, where σ is the surface tension, ρ is the density of the fluid, and g is gravity. For our system the critical power would be $P_0 = 13.5$ W. Our observed threshold, as evident in Fig. 2, is much less: $P_0 = 5.6$ W (1.7 W) for 1.63 Hz (1.82 Hz) and is nonlinearly dependent on the frequency.

The convection-diffusion equation

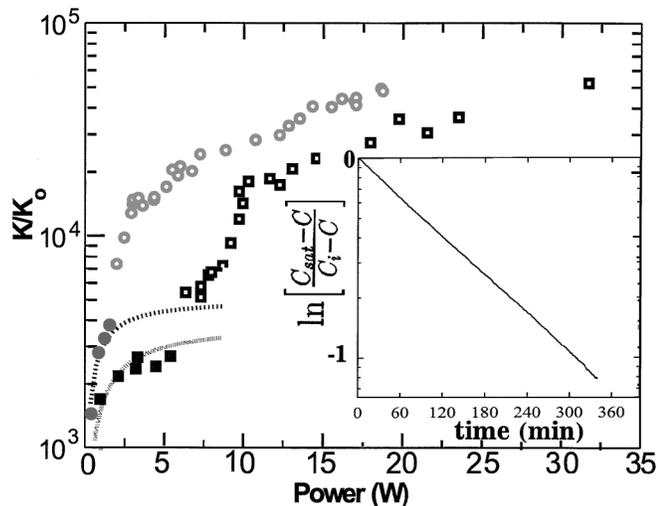$$\frac{\partial C}{\partial t} + \vec{U} \cdot \vec{\nabla} C = D_0 \nabla^2 C \tag{1}$$

FIG. 2. Mass transfer rates versus power to the driving plungers for two different driving frequencies. Solid symbols are simply connected (nonbreaking waves) and open symbols are multiply connected (breaking waves) states, at ($\square$) 1.63 Hz and ($\bigcirc$) 1.82 Hz. The lines are model effective rates (see text) $K/K_0 = \text{Re}^\gamma$, where γ is 0.73. The inset shows the measured O_2 concentration time dependence for a power of 21 W.

governs gas transport, where C is the concentration of dissolved gas, $\vec{U}$ is the velocity field of the liquid, and D_0 is the diffusivity of the gas in the liquid [9]. For O_2 in water D_0 is 2.2×10^{-9} m^2/s at 22 °C [10]. Care must be taken in solving Eq. (1) because the free surface of the fluid, where the concentration must reach saturation, is dynamic and can have a complex topology. Solution of Eq. (1) requires a detailed knowledge of both the velocity field and the shape of the fluid surface. For both complicated velocity fields and complex free surface topologies, the convection-diffusion equation is, for practical purposes, intractable. Empirically, however, the convection-diffusion equation can be reduced to a simple equation called the mass transfer equation [6,10,11]

$$\frac{dC}{dt} = \frac{K}{h}[C_{\text{sat}} - C], \tag{2}$$

where C is the bulk gas concentration, h is the depth of the fluid, and C_{sat} is the concentration at saturation. The parameter K, called the mass transfer coefficient, can then be used to characterize the rate of aeration for both simply and multiply connected wave states, assuming that the measurement is below $\tilde{z}$. A typical measurement of the concentration C is presented in the inset in Fig. 2 and shows an exponential return toward saturation. As the figure shows and our other measurements support, Eq. (2) provides a good description of the ingassing rate. The mass transfer coefficient K is therefore a good global characterization of the ingassing process.

Note that when $\vec{U} = 0$, $K_0 = D_0/h$. In our experiment K_0 for O_2 is 2×10^{-9} m/s. At this rate, it would take over six years for the water tank to become aerated. When there is a wave state ($\vec{U} \neq 0$), the mass transfer coefficient in both capillary [3,4] and gravity wave states (see Fig. 2) is larger than K_0 by many orders of magnitude. This increase cannot be accounted for [3] by simple considerations such as the increased surface area created by the waves. The waves and their associated velocity fields contribute to the aeration in three principle ways: by increasing the surface area (often with bubbles), by providing transport and mixing of aerated fluid from the surface to the fluid bulk, and by thinning the highly aerated surface boundary layer. As in Fig. 2, we first measure values of K, for a given frequency, as a function of our control parameter, the driving power. The value of K, for each input power, is determined from a time series of the dissolved oxygen concentration. We then characterize the wave states for each power and frequency from time series of both their center amplitudes and acoustic emission. By comparison of these quantities we endeavor to quantitatively determine the influence of each of the above effects.

Let us first consider the dependence of the mass transfer coefficient K for simply connected states where wave breaking has no influence. The Reynolds number, Re $= Vd/\nu$, of a flow provides an intrinsic characterization of a system's inertial nonlinearity (where V and d are, respectively, typical velocity and size scales and ν is the

kinematic viscosity). Using characteristic scales for velocity af and length λ, where a is the amplitude of the wave at the center of the tank and λ is the wavelength of the excited state, we find that the simply connected states span $4000 < \mathrm{Re} < 70\,000$. At these Reynolds numbers the flow is turbulent. For a similar range of Re, Tam and Swinney [12] found that for weakly turbulent Taylor-Couette flow passive scalar transport could be described by an effective diffusion equation where the effective turbulent diffusivity D_{eff} could be described as

$$D_{\mathrm{eff}} = D_0 \mathrm{Re}^\gamma \qquad (0.69 < \gamma < 0.83). \qquad (3)$$

Using this relation as a model, we form an effective mass transfer coefficient K:

$$K = K_0 \mathrm{Re}^\gamma. \qquad (4)$$

This relationship is plotted with the experimental data in Fig. 2 and is consistent with the data for the nonbreaking wave states. This model also fits experimental data for simply connected capillary waves [3]. Thus, we conclude that until breaking waves occur, the primary role of the wave state is to provide a means for transport and mixing of the surface layer, via turbulence in the bulk.

Once wave breaking occurs, the ingassing rate jumps, and this model does not adequately describe the observed rates. The induced change in surface topology now begins to play a dominant role in O_2 absorption. To quantitatively characterize the wave states in the system and to relate the changes in the surface topology to the underlying dynamics of the velocity field, we use the wave height sensor and make acoustic measurements. The wave height measurements correlate well, for both simply connected and breaking waves, with pressure changes measured in the liquid bulk using a hydrophone. In the simply connected states, sharp symmetrically spaced sidebands, centered around the main and higher harmonics in the wave height amplitude, appear in the wave height power spectra beyond a critical power threshold. The sidebands in the wave height are *not* subharmonics of the main driving frequency and appear to be related to Benjamin-Feir instabilities [13]. Their appearance (Fig. 3b), although signaling a qualitative change in the wave dynamics, does not have a strong effect on the O_2 absorption rates. As the power is increased, the spectrum broadens and the sharp sidebands disappear. The transition to a broadband spectrum (Fig. 3c) occurs at 5.6 W (1.7 W) for 1.63 Hz (1.82 Hz) and coincides with the onset of wave breaking, as confirmed by the appearance of distinct, high-energy events in the acoustic measurements as made by a microphone above the wave tank (Fig. 4a).

This wave breaking mediated transition to a broadband spectrum coincides [Fig. 3 (right)] with a large increase in ingassing rates. Surprisingly, at higher powers (Fig. 3d) the intensity of the broadband features diminishes. This decrease in broadband power suggests a suppression of the Benjamin-Feir mechanism. This reorganization of the broadband structure [Fig. 3 (right)] corresponds to a sig-
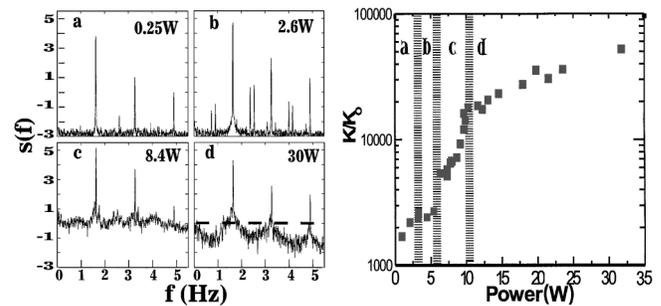

FIG. 3. Left: The power spectral density of wave height at four different powers at a driving frequency of 1.63 Hz. As the power is increased one can see that the fundamental and higher harmonics develop sidebands. At higher power a cascade of sidebands appears, leading toward broadband features. Then, at increased power a reorganization of the broadband spectrum appears. Right: Mass transfer rate versus power into the plungers. Lines indicate the transitions that occur on the left. Waves start to break at (c) and fully developed wave breaking occurs at (d).

nificant reduction of the slope of the K/K_0 versus power input curve.

The onset of high amplitude acoustic events is correlated with the onsets of wave breaking and broadband spectra in the wave height. There is also a corresponding increase in O_2 absorption rates. Consider the mechanisms that lead to these acoustic events. When wave breaking occurs on the fluid surface, pockets of air are enveloped by the crashing wave. These pockets are then broken up into bubbles within the body of the fluid. The bubbles, excited by the dynamics of their creation, then oscillate. At the onset of wave breaking (Fig. 4b) the acoustic signatures of single breaking events are discrete and isolated. Where wave breaking is well developed (Fig. 4c), many high-amplitude, overlapping acoustic events which suggest the creation of a large number of bubbles are observed. The dependence of sound pressure (I_{acoustic}) on power (W) has a comparable trend to K/K_0 (see Fig. 4a). This suggests a relationship between I_{acoustic} and K.

We now relate these measurements to the gas transfer rate. We expect that the creation of bubbles enhances K by the creation of additional surface area and by the enhanced diffusion at the bubble's surface due to increased pressure within the bubble. As the power to our system is increased, the rms acoustic pressure of breaking events, I, also increases. Instead of individual acoustic events that occur at every period in the center of the tank, events at higher power now occur continuously over the entire fluid surface (Fig. 4c). We measure I by averaging the instantaneous absolute acoustic pressure over a time $t \gg f^{-1}$. The acoustic pressure provides an excellent *quantitative* measure of K. Using these data we, empirically, determine a transfer function

$$K = K_0 \left[\mathrm{Re}^\gamma + n\ell\, \frac{I}{\sigma} \right], \qquad (5)$$

where σ is the surface tension, ℓ is the distance from the microphone to the fluid surface, and n is a nondimensional
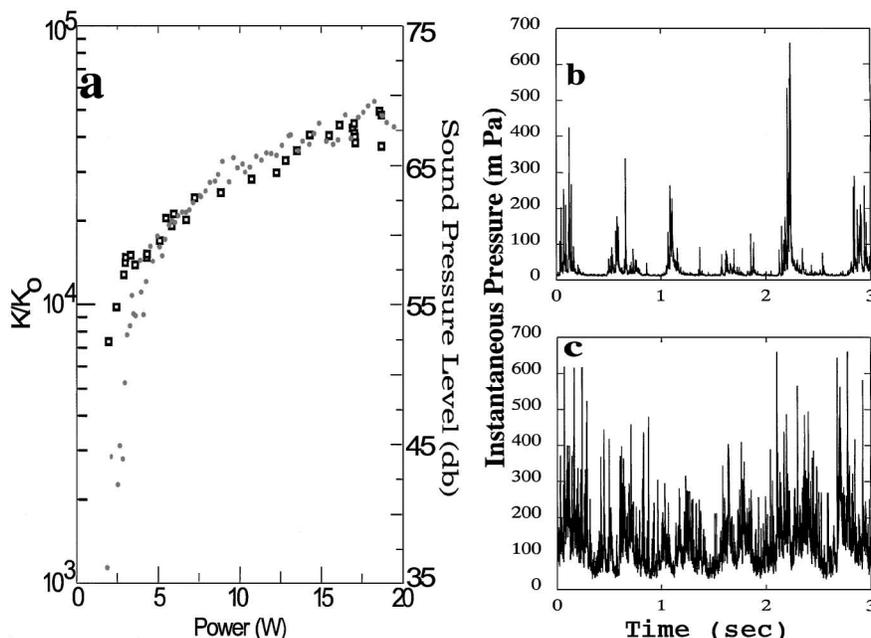
FIG. 4. (a) Mass transfer coefficient ($\square$) and sound pressure level [14] ($\bigcirc$) shown for different power levels in 1.82 Hz waves. Acoustic pressures versus time for (b) isolated breaking events at $P = 4$ W and (c) well-developed breaking at $P = 17.6$ W.

prefactor (here $n = 2.8 \times 10^5$). In Fig. 5 we use this transfer function derived from 1.82 Hz data to provide a *quantitative* prediction for the mass transfer coefficient measured for the 1.63 Hz states. This is particularly significant since, as shown in Fig. 1, the wave states resulting from the two resonances are qualitatively quite different. We suggest that a functional dependence between K and I can provide oceanographers with a means to use remote sensing techniques to estimate mass transfer coefficients in the field. This suggestion needs to be followed by other tests for progressive waves and waves with surfactants.
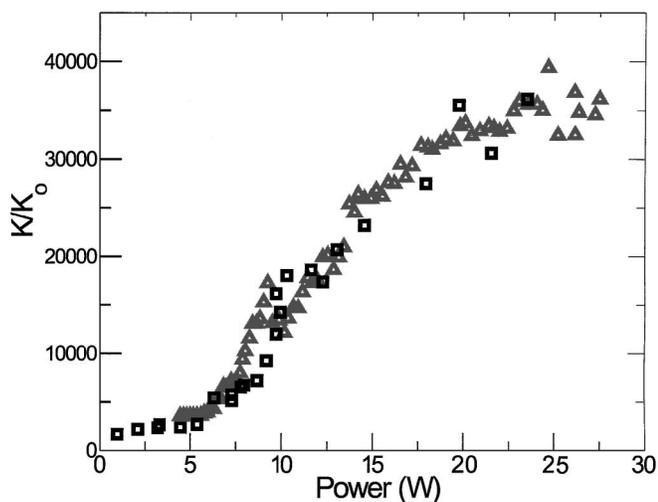

FIG. 5. Mass transfer rates versus power at frequency $f = 1.63$ Hz. Measured K/K_0 ($\square$) compared to predicted K/K_0 ($\triangle$) using a transfer function relating acoustic pressure as derived from data at 1.82 Hz [Eq. (5)].

[1] G. Asra and J. Dozier, *EOS Science Strategy for the Earth Observing System* (AIP Press, New York, 1994).

[2] J. L. Sarmiento and C. L. Quéré, Science **274**, 1346 (1996); P. F. Hoffman, A. J. Kaufman, G. P. Halverson, and D. P. Schrag, Science **281**, 1342 (1998).

[3] J. R. Saylor and R. A. Handler, Phys. Fluids **9**, 2539 (1997).

[4] B. Jähne and H. Haußeker, Annu. Rev. Fluid Mech. **30**, 443 (1998).

[5] B. Jähne, K. Otto, R. Bö, A. Dutzi, W. Huber, and P. Libner, J. Geophys. Res. **92**, 1937 (1987).

[6] A. L. Downing and G. A. Truesdale, J. Appl. Chem. **5**, 570 (1955).

[7] W. E. Aferoff and R. Wanninkhof, J. Geophys. Res. **103**, 10 555 (1998).

[8] A. C. Newell and V. E. Zakharov, Phys. Rev. Lett. **69**, 1149 (1992).

[9] A. J. Szeri, J. Fluid Mech. **332**, 341 (1997).

[10] H. Chanson, *Air Bubble Entrainment in Free-Surface Turbulent Shear Flows* (Academic Press, London, 1996).

[11] S. J. Arceivala, *Wastewater Treatment and Disposal* (Marcel Dekker, Inc., New York, 1982).

[12] W. Y. Tam and H. L. Swinney, Phys. Rev. A **36**, 1374 (1987).

[13] J. T. Stuart and R. C. DiPrima, Proc. R. Soc. London A **362**, 27 (1978).

[14] The sound pressure level is defined as (db) $= 20 \log(I/I_0)$. I_0 is taken as 28.9 μPa.